A Peptidomimetic Antibiotic Interacts with the Periplasmic Domain of LptD from Pseudomonas aeruginosa

Andolina, Gloria ; Bencze, László-Csaba ; Zerbe, Katja ; Müller, Maik ; Steinmann, Jessica ; Kocherla, Harsha ; Mondal, Milon ; Sobek, Jens ; Moehle, Kerstin ; Malojčić, Goran ; Wollscheid, Bernd ; Robinson, John A

Abstract: The outer membrane (OM) in Gram-negative bacteria is an asymmetric bilayer with mostly lipopolysaccharide (LPS) molecules in the outer leaflet. During OM biogenesis, new LPS molecules are transported from their site of assembly on the inner membrane to the OM by seven LPS transport proteins (LptA-G). The complex formed between the integral -barrel OM protein LptD and the lipoprotein LptE is responsible for transporting LPS from the periplasmic side of the OM to its final location on the cell surface. Because of its essential function in many Gram-negative bacteria, the LPS transport pathway is an interesting target for the development of new antibiotics. A family of macrocyclic peptidomimetics was discovered recently that target LptD and inhibit LPS transport specifically in Pseudomonas spp. The related molecule Murepavadin is in clinical development for the treatment of life-threatening infections caused by P. aeruginosa. To characterize the interaction of these antibiotics with LptD from P. aeruginosa, we characterized the binding site by cross-linking to a photolabeling probe. We used a hypothesis-free mass spectrometry-based proteomic approach to provide evidence that the antibiotic cross-links to the periplasmic segment of LptD, containing a -jellyroll domain and an N-terminal insert domain characteristic of Pseudomonas spp. Binding of the antibiotic to the periplasmic segment is expected to block LPS transport, consistent with the proposed mode of action and observed specificity of these antibiotics. These insights may prove valuable for the discovery of new antibiotics targeting the LPS transport pathway in other Gram-negative bacteria.

DOI: https://doi.org/10.1021/acschembio.7b00822

A Peptidomimetic Antibiotic Interacts with the Periplasmic Domain of LptD from *Pseudomonas aeruginosa*

Gloria Andolina[#1,2], László-Csaba Bencze[#1,3], Katja Zerbe[#], Maik Müller[+], Jessica Steinmann[#], Harsha Kocherla[#], Milon Mondal[#], Jens Sobek[⊗], Kerstin Moehle[#], Goran Malojčić[‡,4], Bernd Wollscheid[+] and John A. Robinson[#5]

[#] Chemistry Department, University of Zurich, Winterthurerstrasse 190, 8057 Zurich, Switzerland.

[+] Institute of Molecular Systems Biology, Department of Health Sciences and Technology, ETH Zürich, Auguste-Piccard-Hof 1, 8093 Zürich, Switzerland.

[‡] Department of Chemistry and Chemical Biology, Harvard University, 12 Oxford Street, Cambridge, MA 02138, USA.

[⊗]Functional Genomics Center Zurich, Winterthurerstrasse 190, 8057 Zurich, Switzerland.

[1] Both authors contributed equally to this work.

[2] Current address: Department of Chemistry, University of Hong Kong, Pokfulam Road, Hong Kong.

[3] Current address: Department of Chemistry, Babeș-Bolyai University, Cluj-Napoca 400084, Romania.

[4] Current address: Goldfinch Bio, 215 First Street, 4th Floor, Cambridge, MA 02142, USA.

[5] To whom correspondence should be addressed: Chemistry Dept., University of Zurich, 8057 Zurich, Switzerland, Tel.: 41-44-635-4242; E-mail: john.robinson@chem.uzh.ch

Abstract

The outer membrane (OM) in Gram-negative bacteria is an asymmetric bilayer with mostly lipopolysaccharide (LPS) molecules in the outer leaflet. During OM biogenesis, new LPS molecules are transported from their site of assembly on the inner membrane to the OM by seven LPS transport proteins (LptA-G). The complex formed between the integral ß-barrel OM protein LptD and the lipoprotein LptE is responsible for transporting LPS from the periplasmic side of the OM to its final location on the cell surface. Because of its essential function in many Gram-negative bacteria, the LPS transport pathway is an interesting target for the development of new antibiotics. A family of macrocyclic peptidomimetics was discovered recently that target LptD and inhibit LPS transport specifically in *Pseudomonas* spp. The related molecule Murepavadin is in clinical development for the treatment of life-threatening infections caused by *P. aeruginosa*. To characterize the interaction of these antibiotics with LptD from *P. aeruginosa*, we characterized the binding site by crosslinking to a photolabeling probe. We used a hypothesis-free mass spectrometry-based proteomic approach to provide evidence that the antibiotic cross-links to the periplasmic segment of LptD, containing a ß-jellyroll domain and an N-terminal insert domain characteristic of *Pseudomonas* spp. Binding of the antibiotic to the periplasmic segment is expected to block LPS transport, consistent with the proposed mode of action and observed specificity of these antibiotics. These insights may prove valuable for the discovery of new antibiotics targeting the LPS transport pathway in other Gram-negative bacteria.

Introduction

According to the World Health Organization,[1] Gram-negative bacterial infections are causing increasing levels of morbidity due to the rise of resistance to established antibiotics, particularly in *Pseudomonas*, *Acinetobacter* and various Enterobacteriacea species.[2] However, few new antibiotic classes have been discovered recently to combat Gram-negative bacterial infections. A target of special interest in this context is the Gram-negative bacterial outer membrane (OM), consisting of an asymmetric bilayer with lipopolysaccharide (LPS) in the outer leaflet and membrane phospholipids in the inner leaflet.[3] During OM biogenesis, the glycolipid LPS molecules are assembled in the cytoplasm and at the inner membrane (IM),[4] before being transported across the periplasm and integrated into the outer leaflet by seven essential LPS transport proteins (LptA–LptG), which assemble into a complex spanning the entire envelope (Figure 1A).[5] At the IM, the $LptFGB_2$ complex extracts LPS molecules from the IM, before transport to the OM across a bridge formed by multiple copies of LptA.[6,7] The LptA bridge thus connects the IM and OM, and provides a pathway for shuttling LPS molecules to a complex in the OM comprising the integral ß-barrel membrane protein LptD and the lipoprotein LptE.[8] In the final step, the LptD/E complex translocates LPS from the periplasmic side of the OM into the outer leaflet and the cell surface.[9]

According to the PEZ-model of LPS transport,[5,10] ATP hydrolysis catalyzed by the $LptFGB_2$ complex, first drives extraction of LPS from the inner membrane and then pumps LPS across the LptA bridge and onto the cell surface. The lipid chains of LPS remain anchored in V-shaped hydrophobic cavities within the jellyroll domain of first LptC, then LptA,[11] and finally the jellyroll domain within the N-terminal periplasmic segment of LptD (Figure 1A).[8] The C-terminal domain of LptD, comprising a 26-stranded ß-barrel, is integrated in the OM, with the lipoprotein LptE bound within the lumen of the ß-barrel.[12-14] One side of the LptD ß-barrel may transiently accommodate the LPS sugar chain as it reorients vertically on its way to the cell surface.[15] The lipid A portion of LPS is thought to emerge into the outer leaflet through a transient opening in the side of the LptD ß-barrel.[10] Several crystal structures of recombinant LptD/E from different Gram-negative bacteria have been reported recently.[16] However, the complex is clearly a highly dynamic machine that shuttles through many different conformational states during OM biogenesis.

Due to its essential role in OM biogenesis, and exposed location on the cell surface, LptD/E has become an interesting target in antibiotic discovery. Amongst the growing interest

in naturally occurring host defense peptides and peptidomimetic antibiotics,[17,18] a family of synthetic macrocyclic ß-hairpin antibiotics including **L27-11** (Figure 1B) was described recently, which target LptD/E and inhibit LPS transport in *Pseudomonas* spp.[19-22] Photochemical cross-linking studies showed that the antibiotics bind with high selectivity to LptD in the OM of *P. aeruginosa (Pa)*.[19] An important insight into the mode of action came with the isolation of spontaneously resistant *Pa* strains containing a mutation (a six-residue tandem duplication) in the periplasmic ß-jellyroll domain of LptD. This mutation confers resistance and blocks binding of the antibiotic to LptD.[19] However, understanding the mode of action and specificity towards *Pseudomonas* spp. requires a more detailed analysis of the antibiotic binding site. In this work, we set out to identify the domain of LptD that mediates binding to **L27-11**, through analysis of site(s) of photo-crosslinking to a related photoprobe called **PAL6**. Understanding how these peptidomimetics interact with pseudomonas LptD/E could aid the discovery of new antibiotics targeting LptD in other Gram-negative bacteria. Already a closely related clinical candidate called Murepavadin (also called **POL7080**) has been developed by *Polyphor* AG as a pseudomonas-specific antibiotic.[23] Murepavadin recently completed successfully phase-II clinical tests in hospital patients with life-threatening pseudomonas lung infections (clinical trials identifier NCT02096328).

Results and discussion

Production and characterization of *Pa* LptD/E$_{His}$

Pa LptD/E$_{His}$ was produced in *E. coli* (*Ec*) using established procedures, by introducing genes for full-length LptD and a His-tagged LptE into an *E. coli* host (Figure 2A).[12-14,24,25] The *Pa* LptD/E$_{His}$ complex could be isolated by Ni-affinity chromatography, which provides strong prima facie evidence for formation of a natively folded ß-barrel domain in *Pa* LptD, able to form a stable complex with *Pa* LptE. SDS-PAGE of the purified complex, after heat denaturation to dissociate LptD from LptE, and in the presence of reducing agent (DTT), shows two Coomassie-stained bands at the expected masses (Figure 2B). To investigate the redox status of disulfide bonds, the mobility of heat-denatured protein in polyacrylamide gels was examined further.

Ec LptD (residues 25–784; signal peptide 1–24) can form two disulfides between four non-consecutive cysteine residues (Figure 2A), and at least one disulfide must be present in

order for LptD to function in LPS transport.[26] After heat denaturation by boiling to dissociate the complex, the mobility of LptD in gels changes in a manner characteristic of the oxidation state of these disulfide bonds linking the jellyroll domain to the ß-barrel domain.[26,27] Reduced and denatured *Ec* LptD ($LptD_{RED}$) migrates faster at ≈90 kDa, whereas non-reduced LptD containing at least one interdomain disulfide ($LptD_{OX}$) linking the periplasmic segment to the ß-barrel, migrates more slowly at ≈110 kDa.[24] *Pa* LptD is larger (34–924 residues, ≈100 kDa) and contains six cysteines, including four that are likely to form disulfides analogous to those seen in *Ec* LptD (see below and Figure 2A). The periplasmic segment of *Pa* LptD (res. 34–323) comprises not only a jellyroll domain, similar to that present in *Ec* LptD, but also an additional ≈100 residue domain found in LptD from pseudomonads, and in very few other Gram-negative bacteria. This insert domain also contains a pair of cysteine residues that might form a disulfide, as indicated in Figure 2A.

The mobility of heat denatured *Pa* LptD in SDS-PAGE was analyzed with and without reduction with DTT. Both the recombinant *Pa* $LptD/E_{His}$ extracted from *Ec* and wild-type *Pa* LptD/E extracted from *Pa* PAO1 membranes, behaved similarly on SDS-PAGE (Figure 2C), with the denatured and non-reduced LptD migrating with apparent size ≈130 kDa and the reduced form (with DTT) with apparent size ≈100 kDa. These results suggest that putative interdomain disulfides are present both *in vivo* and *in vitro*, linking the ß-barrel to the periplasmic segment in *Pa* $LptD/E_{His}$. Further support for this conclusion came by examining the gel mobility of targeted Cys-to-Ser mutants of the *Pa* $LptD/E_{His}$ produced in *E. coli*, in analogy to similar experiments reported earlier for the *Ec* LptD.[26] A mutant *Pa* LptD with all six cysteine residues mutated to serine (*Pa* $LptD_{SSSSSS}$; where SSSSSS signifies the sequential replacement of all six Cys to Ser) could also be purified by Ni-affinity chromatography, and upon heating migrated under both reducing and non-reducing conditions in an SDS-PAGE gel at the position found for $LptD_{RED}$ (≈100 kDa) (Figure 2D). This result parallels that reported for the *Ec* LptD, where eliminating all Cys residues does not significantly destabilize LptD or prevent formation of the LptD/E complex.[26] When two cysteine residues expected to form interdomain disulfides, analogous to those in *Ec* LptD (Figure 2A), are re-introduced (C270/C859 ($LptD_{SSSCSC}$) and C39/C858 ($LptD_{CSSCS}$)) each protein after heating under non-reducing conditions migrated either partly ($LptD_{SSSCSC}$) or fully ($LptD_{CSSCS}$) at ≈130 kDa, whereas the reduced form migrated at ≈100 kDa (Figure 2D). In some assays *Pa* LptD (wt and mutant) showed both 130/100 kDa bands when analyzed under non-reducing conditions (Figure 2D), possibly due to partial reduction of the protein during the cell disruption procedure or incomplete oxidation

in *E. coli*. These results indicate that disulfides homologous to those seen in *Ec* LptD can form in the *Pa* LptD, and that this gel mobility shift assay provides a useful method to monitor the interdomain redox status of the *Pa* LptD/E complex.[26] In summary, these results suggest that the recombinant *Pa* LptD/E_{His} has a native-like fold, like that of LptD/E present in *Pa* membranes.

Binding of antibiotic to *Pa* LptD/E_{His}

Binding of antibiotic **L27-11** to recombinant *Pa* LptD/E_{His} was tested using two different biophysical methods, surface plasmon resonance (SPR, *GE Healthcare*) and microscale thermophoresis (MST, *Nanotemper Technologies*). For SPR studies, the protein was immobilized through a Ni-NTA ligand, covalently linked to the biosensor surface, and increasing concentrations of free **L27-11** were eluted over this surface. Association and dissociation kinetics fast on the SPR timescale were observed (Figure 3A), so equilibrium responses were analyzed with a Langmuir binding model, which gave an apparent K_D of 32 ± 10 nM for the interaction. A binding isotherm could also be detected by MST with both components now free in solution (Figure 3B), using the fluorescently labeled derivative **fl-L27-11** (Figure 4). Titrating **fl-L27-11** with LptD/E_{His} gave a low but reproducible response, and an apparent $K_D \approx 13 \pm 5$ nM for the interaction. The enantiomer of **L27-11** (**ent-L27-11**) shows no antimicrobial activity against *Pa*.[19] As a control, therefore, binding of **ent-L27-11** was monitored to fluorescently labeled LptD/E_{His} by MST. However, a binding isotherm could only be detected at peptide concentrations ≈1000x higher than seen for **L27-11**. We conclude that the recombinant *Pa* LptD/E_{His} complex retains an ability to bind enantioselectively the peptidomimetic antibiotic *in vitro*, in a concentration range similar to the observed antimicrobial activity of **L27-11**,[19] although the MIC reflects inhibition of growth and not a binding reaction.

Trypsin digestion of *Pa* LptD/E_{His}

Folded ß-barrel proteins are often thermally stable and resistant to trypsin digestion. The reported trypsin digestion of *Ec* LptD leads to release of a ≈62 kDa trypsin resistant fragment starting at F203, close to the start of the C-terminal ß-barrel domain (Figure 2A).[24] When the *Pa* LptD/E_{His} was partially digested with trypsin, two fragments could be readily detected by

SDS-PAGE, one at ≈95 kDa (fragment F1) and another at ≈70 kDa (fragment F2) (Figure 5A). N-terminal Edman sequencing revealed that fragment F1 arises by trypsin cleavage at R107, whereas fragment F2 arises by cleavage at R301. Only the F1 fragment is recognized in Western blotting by polyclonal anti-LptD antiserum raised against the C-terminal 20 residues, likely due to loss through proteolysis in F2 of the C-terminal segment including the antibody epitope. This C-terminal segment (res. 895–924) follows the last ß-strand and so is not an integral part of the ß-barrel. R107 lies within the predicted insert domain (Figure 2A), whereas R301 lies close to the start of the ß-barrel domain.

Photolabeling experiments

For photolabeling experiments, the probe **PAL6** was developed (Figure 4). Compared to **L27-11**, **PAL6** contains multiple substitutions of Arg/Lys residues (Figure 1B) for diaminobutyric acid (Dab), with the result that the macrocyclic peptide is much more stable to proteolysis by trypsin.[19,21] **PAL6** retains, however, potent antimicrobial activity (MIC against *Pa* PAO1 ≈ 0.03 μg/mL in MH-II broth).

In vivo photolabeling of whole *Pa* cells by **PAL6** showed highly selective labeling of LptD by Western blotting (Figure 5B). Upon trypsin digestion of *Pa* LptD/E extracted from *Pa* membranes, the formation of the F1 fragment (≈95 kDa) was detected in a Coomassie-stained gel, and was confirmed by in-gel trypsin digestion and tandem mass spectrometry (MS/MS) analysis of fragments, as well as by reaction with anti-LptD antibodies recognizing the C-terminal 20 residues (Figure 5B/C). Importantly, however, the F1 fragment gave no signal upon biotin detection, showing that the F1 fragment has lost the biotin tag, and therefore the site of photo-crosslinking.

In vitro photolabeling of *Pa* LptD/E_{His} by **PAL6** also showed highly selective labeling of LptD by Western blotting (Figure 5D/E). Upon trypsin digestion, the formation of the F1 fragment (≈95 kDa) was detected in a Coomassie-stained gel, and was confirmed by in-gel trypsin digestion and tandem mass spectrometry (MS/MS) analysis of fragments, as well as by reaction with anti-LptD antibodies recognizing the C-terminal 20 residues. However, the F1 fragment now retains a strong signal upon biotin detection (Figure 5C/D), showing that this fragment contains covalently attached photoprobe. However, no biotin signal was detected in the F2 fragment, suggesting that the ß-barrel is not labeled by the photoprobe. Attempts to

directly detect smaller biotinylated peptides using this Western blotting approach gave inconclusive results. A more detailed analysis was therefore undertaken using a mass spectrometry-based approach.

Detection of photolabeled fragments by mass spectrometry

The photolabeling by **PAL6** of recombinant *Pa* LptD/E_{His} was analyzed by quantitative MS-based proteomics, which starts with the assumption that photo-crosslinking of **PAL6** to LptD/E_{His} results in covalent attachment of the photoprobe to one or more spatially proximal amino acids, in or close to the antibiotic binding site. Compared to unlabeled protein, **PAL6** labeled peptides obtained upon proteolytic digestion are then less likely to be detected by MS, due to altered peptide precursor mass, fragmentation patterns and ionization efficiency. Thus, comparing peptide abundances between **PAL6**-labeled and unlabeled LptD/E_{His} digests, permits the identification of **PAL6** modified regions in a hypothesis-free fashion.

Comprehensive detection of LptD and LptE_{His} peptides across structural domains by MS is a prerequisite for the unbiased identification of **PAL6** binding sites. Thus, we first optimized proteolytic digestion and MS detection of LptD/E_{His}-derived peptides. For this, equal amount of **PAL6**-labeled and unlabeled LptD/E_{His} protein was reduced and sequentially digested under denaturing conditions with a mix of proteolytic enzymes consisting of Lys-C, trypsin and chymotrypsin. A small aliquot of each sample was pooled and analyzed by HPLC-MS/MS in data-dependent acquisition (DDA) mode for sensitive and discovery-driven identification of proteolytic peptides. A peptide search using a database containing pseudomonas LptD/E protein sequences led to identification of 409 and 80 peptides (false discovery rate (FDR) < 0.01), representing a sequence coverage of 85% and 81% for LptD and LptE_{His}, respectively (Table S2 and Figure S4). Although, folded ß-barrel proteins are often resistant to trypsin digestion, the identified proteolytic peptides of LptD originate from its insert, jellyroll as well as ß-barrel domain. This indicates comprehensive and structure independent coverage of LptD/E_{His} by MS under optimized conditions.

To identify potential **PAL6** binding sites, MS detectable peptides were analyzed for an altered abundance upon **PAL6** photo-crosslinking. For this, **PAL6**-photolabeled and unlabeled LptD/E_{His} protein digests were analyzed by HPLC-MS/MS in data-independent acquisition (DIA) mode for label-free quantification of LptD/E_{His} derived peptides. Peptides were quantified

by integration of associated fragment-ion traces. Data analysis using Spectronaut software (*Biognosys*, Schlieren) allowed relative quantification of 335 peptides with unique amino acid sequences, 280 of which could be assigned to LptD and 55 to $LptE_{His}$ (Table S2). Thirty-six peptides were significantly down-regulated upon **PAL6** photo-crosslinking (fold change of > 1.5 and q-value < 0.05) and all of them stem from LptD (Figure 6). A cluster including most significantly regulated peptides maps to the β-jellyroll region of LptD and shares the unique amino acid sequence "ENR" (res. 199–201). Additionally, a second population of peptides significantly affected by **PAL6** photo-crosslinking maps to the insert domain of LptD and comprises the sequence stretch "ETV" (res. 85–87). From this we conclude that **PAL6** preferentially binds to the periplasmic region of recombinant $LptD/E_{His}$ *in vitro*, and more specifically, to defined segments within the β-jellyroll and the pseudomonas-specific insert domain of LptD.

Discussion

The peptidomimetic **L27-11** (Figure 1) is a potent antibiotic acting specifically against *Pseudomonas* spp., and a related photoprobe was shown earlier to photolabel LptD with high selectivity in whole cells of *P. aeruginosa (Pa)*.[19] In this work, *in vivo* photolabeling of *Pa* PAO1 with the photoprobe **PAL6** also leads to highly selective labeling of LptD (Figure 5B). However, the low natural abundance of LptD in *Pa* and the poor efficiency of photochemical cross-linking with this photoprobe, are major obstacles in efforts to analyze the site(s) of *in vivo* photolabeling in this large membrane protein. Furthermore, the carbene photochemically-generated from **PAL6** can also undergo fast internal quenching by 1,2-H-shift, which lowers significantly the cross-linking efficiency. Before discussing the sites of photo-crosslinking by **PAL6**, we first discuss in more detail the known structures of LptD from various Gram-negative bacteria and the likely domain organization of *Pa* LptD.

As indicated in Figure 2, *Ec* LptD comprises a C-terminal ß-barrel domain and an N-terminal periplasmic domain of ≈200 residues (see also Figure 1C). The *Ec* LptD contains four Cys residues that form two disulfide bonds linking the barrel domain with the jellyroll domain, which are required for the proper function of the transporter.[24,26,27] Crystal structures are available of full-length LptD/E from *Shigella flexneri* (PDB 4Q35) (shown in Figure 1C), which has very high sequence identity to the *Ec* LptD, as well as *Klebsiella pneumoniae* (5IV9).[13,14] Both

structures include the LptD transmembrane ß-barrel and the complete N-terminal periplasmic segment with its ß-jellyroll domain. In addition, structures of truncated forms of LptD, lacking the entire N-terminal periplasmic segment are available for LptD/E from *Salmonella enterica* (4N4R),[12] *P. aeruginosa* (5IVA),[14] *Escherichia coli* (4RHB) (to be published), *Klebsiella pneumoniae* (5IV8)[14] and *Yersina pestis* (5IXM).[14] In all these crystal structures, the 26-stranded LptD ß-barrel domain is highly conserved and the lumen of the barrel is plugged in each case by LptE. However, the crystal structure of full-length *Pa* LptD/E with the periplasmic domain has not yet been reported. In *Pseudomonas* spp., the periplasmic segment of LptD is significantly longer than that in most other γ-proteobacteria, due to the presence of an additional N-terminal ≈100 residue "insert" domain of unknown structure and function (res. 45–144) (Figure 2A). The *Pa* ß-jellyroll domain is similar in sequence (similarity 47%; identity 28%) to that in *Shigella flexneri* LptD (Table S1), suggesting a similar ß-jellyroll fold (res. 145-323). Based upon a sequence alignment, a homology model for the jellyroll in *Pa* LptD could be generated (see Supporting Information). The relative orientation of the ß-jellyroll and β-barrel domain in *Pa* LptD could be very similar to that in the full-length *Sf* LptD crystal structure. In particular, the sequences of the region linking the ß-jellyroll to the barrel in *Pa* LptD (I317–L326) and *Shigella flexneri* (V220–L229) contain conserved residues, indicating a similar fold in this region. For the insert domain, a sequence motif search in the PDB database revealed low sequence similarities with parts of a human V_H Ig-like domain (PDB 1T2J). Ig-like domains are frequently found in *E. coli* cell surface proteins, where they play various roles in host cell adhesion and invasion by pathogenic strains.[28] A homology model of the *Pa* insert domain with a truncated Ig-like fold could also be generated (see Supporting Information).[28] However, this model is speculative, and it is currently unclear how the individual domains within the periplasmic segment (insert, ß-jellyroll and ß-barrel) are arranged in 3D space. As discussed below, the photolabeling experiments provide clear evidence that the antibiotic binds to the periplasmic portion of LptD, but without structural information it is not yet possible to analyze the likely binding site in terms of 3D structures (*vide infra*).

The first information about possible sites of *in vivo* photo-crosslinking of **PAL6** to *Pa* LptD could be obtained by exploiting highly sensitive biotin detection in Western blotting of trypsin fragments derived from photolabeled LptD (Figure 5B/C). Crosslinking of **PAL6** occurs to a segment of the periplasmic insert domain (res. 34-107) that is cleaved from the F1 fragment by trypsin. No evidence was obtained for labeling of the ß-barrel domain in LptD. For analysis of *in vitro* photo-crosslinking, a quantitative mass spectrometry-based proteomics

approach could be used, which identifies differences in abundance of proteolytic peptide fragments derived from labeled versus unlabeled LptD. This approach avoids problems that arise when attempting to directly and comprehensively detect labeled protein fragments by MS, due to uncertain mass shifts and ion-suppression effects that occur with modified peptide fragments. Rather, a hypothesis-free approach was taken here to map in one experiment all fragments of the protein that are modified by the photoprobe. The results obtained illustrate the potential of the approach as a method for mapping ligand-receptor binding sites. The MS results show that cross-linking occurs *in vitro* to two sites in LptD, one around res. 85–87 (ETV) in the insert domain, and another within the ß-jellyroll domain around residues 199–201 (ENR) (Figure 6).

Whereas *in vitro* labeling around res. 85-87 in the insert domain is consistent with the observations made for *in vivo* labeling, the second site of *in vitro* cross-linking around res. 199-201 was not detected in the *in vivo* photolabeling experiments. We conclude, therefore, that although a native-like fold exists *in vitro*, there must be some differences between the antibiotic binding site in LptD detected by photolabeling *in vitro* and *in vivo*. We hypothesize that this may be due to the different environments experienced by the LptD/E complex. For example, *in vivo* the protein is integrated into a membrane bilayer and may be shuttling between different conformational states during LPS transport, whereas *in vitro* the LptD/E_{His} complex is solubilized in a detergent micelle. Recent studies, for example, have shown for one ß-barrel protein (OmpX) that while it forms a stable ß-barrel in detergent micelles, bicelles and nanodiscs, the dynamics of the protein differ substantially between the detergent and lipid environments.[29] Furthermore, *in vivo* the N-terminal region of LptD, where binding to the antibiotic should occur, is bound to LptA as part of the Lpt transport macromolecular complex. The absence of LptA *in vitro* may also affect the structure or dynamics of this region in LptD. Changes in conformation and/or dynamics of LptD might have a significant effect on the diffusion and site of eventual cross-linking of the reactive carbene generated by photolysis of **PAL6**. Notwithstanding this, we believe that the results presented are important, because they show for the first time that the ß-barrel domain is not labeled, and that both *in vivo* and *in vitro* photolabeling provide evidence for a binding site within the periplasmic segment of LptD.

As mentioned earlier, one additional evidence that the antibiotic binding site is close to the ß-jellyroll domain came from the isolation of a resistant mutant of *Pa*, containing a six-residue tandem duplication at res. 210–215 in LptD.[19] This mutation blocks binding of the

antibiotic to LptD, and maps in a homology model of the jellyroll domain to the tip of a ß-hairpin loop on one side of the V-shaped hydrophobic groove (Figure 7B). Interestingly, on the opposite side of the V-shaped groove in this model lies a hairpin loop containing one of the sites detected by photo-crosslinking (res. 199-201). It is noteworthy that the three sites implicated in antibiotic binding are discontinuous in the primary sequence of the protein (res. 85-87; res. 199-201; res. 210-215), yet folding may bring them close together in the three-dimensional structure of the protein. Multiple attempts were also made here to express the periplasmic segment of *Pa* LptD as a recombinant protein, to facilitate structural studies. However, ^{15}N-labeling of the protein and analysis of amide proton dispersion in ^{15}N-^{1}H 2D-HSQC NMR spectra showed that the recombinant protein could not be obtained in a stable folded form (results not presented).[30] Finally, the unique selectivity and mode of action of the antibiotic for pseudomonads can now be understood in terms of the direct involvement of the LptD periplasmic insert domain in antibiotic binding, and this insert domain is found almost exclusively in the LptD of pseudomonads. The current model for LPS transport proposes that the lipid chains of LPS interact with the hydrophobic groove of the jellyroll domains in LptA and LptD. A molecule that binds in or close to this groove in LptD should therefore be able to interrupt LPS transport, consistent with the proposed mechanism of action.[20] Further progress on this challenging problem will likely require a 3D structure of the periplasmic segment of *Pa* LptD and its complex with bound antibiotic.

METHODS

Production of *Pa* LptD/E in *E. coli*. The *lptD* and *lptE* genes from *P. aeruginosa* (*Pa*) PAO1 (PA0595 and PA3988) were amplified by PCR from genomic DNA (see Supporting Information for primer sequences). *Pa lptD* was cloned into *NdeI*/*BamH1* restriction sites in pET3a (*Novagen*) including its native signal sequence. Upon expression in *E. coli* and cleavage of the signal peptide, LptD has the native N-terminus (res. 34–924) (Figure 2A). *Pa lptE* was cloned into *NcoI*/*XhoI* sites in the pCDFduet-1 vector (*Novagen*) with its native signal sequence. Upon expression in *E. coli*, addition of diacylglycerol to the conserved C20 residue, signal peptide cleavage and N-acylation by the Lnt transacylase,[31] *Pa* LptE is produced with an N-terminal lipid anchor and a C-terminal His_6 tag ($LptE_{His}$). Both plasmids were introduced into *E. coli* BL21 DE3 and simultaneous expression of *Pa* LptD and $LptE_{His}$ was initiated by addition

of IPTG (100 μM) at OD_{600} = 0.6. After cell growth for 16 h at 23°C, an OM preparation was isolated by differential ultracentrifugation and a washing step using 0.5% N-lauroylsarcosine.[32]

The OM pellet was dissolved in PBS (50 mM, pH 7.4) containing 1% (w/v) LDAO and lysozyme (100 μg mL^{-1}), and the *Pa* LptD/E_{His} complex was purified by Ni-affinity chromatography, with elution in buffer containing 300 mM imidazole and 1% n-octyl-ß-D-glucopyranoside (OG). Fractions containing *Pa* LptD/E_{His} were concentrated (50 kDa cut-off filter) and purified by gel filtration on Superdex 200 (PBS buffer with w/v 1% OG). The resulting *Pa* LptD/E_{His} complex shows mainly two bands with the expected apparent masses on Coomassie-stained SDS-PAGE (Figure 2B). An N-terminal amino acid analysis and in-gel trypsin digestion with MS/MS analysis confirmed the identity of the ≈105 kDa band as *Pa* LptD, whereas direct MS confirmed the ≈25 kDa band as *Pa* $LptE_{His}$. Western blotting showed that each protein reacted with complementary IgG antiserum raised against a peptide corresponding to the C-terminal 20 amino acids of LptD (anti-LptD) or the C-terminal 16 residues of *Pa* LptE. The anti-sera do not recognize the corresponding *E. coli* LptD/E upon Western blotting (not shown). Individual site-specific mutants were generated using QuikChange multi-site directed mutagenesis kit (*Agilent*) and produced using the method above.

Trypsin digestion. LptD/E_{His} (100 μg) and sequencing grade trypsin were incubated in PBS buffer with 1% OG at 37°C. Aliquots were removed at time intervals, boiled with SDS-loading buffer, and analyzed by SDS-PAGE (8% gel). The gel was either stained with Coomassie blue, or used for Western blotting (PVDF membrane) for anti-LptD or biotin detection (Figure 5).

Binding studies. For SPR studies a NiHC1000 sensor chip with a BIAcore T100 (*GE Healthcare*) instrument was equilibrated with PBS buffer (pH 7.4, 50 mM) containing 1% w/v OG and loaded with *Pa* LptD/E_{His} (160 nM) to a surface density of ca. 3500 RU. After blocking free Ni-sites with poly-His-tagged peptide, a series of analyte (**L27-11**) concentrations at 0.25–500 nM, in the same buffer, at a flow rate of 20 μL mL^{-1}, were eluted over the biosensor surface at 25°C for 60 s, followed by dissociation without analyte over 180 s. The biosensor surface was regenerated with 100 mM EDTA for 600 s between each run. The entire experiment was repeated in triplicate. For data analysis, a double referencing approach was used with BIAcore T100 evaluation software v. 1.1.1. The steady state response was used to determine a K_D of 32 ± 10 nM (Figure 3A).

Microscale thermophoresis (MST) experiments were performed with a Monolith NT.115 instrument (*NanoTemper Technologies*) with hydrophobic capillaries at room temperature. A dilution series of LptD/E_{His} (5000–0.15 nM) was added to **fl-L27-11** (Figure 4) at 10 nM in PBS buffer (pH 7.4, 50 mM) containing 1% w/v OG. Binding isotherms were generated using NTAffinityAnalysis v2.0.1334 software provided by the manufacturer (Figure 3B). The average K_D from triplicate measurements was 13 ± 5 nM. In addition, binding of **L27-11** and **ent-L27-11** were measured under the same conditions using LptD/E_{His} labelled using a Dylight™ 650-N-hydroxysuccinimide ester labelling kit (*Thermofisher*).

Photolabeling experiments. The photoprobe **PAL6** (Figure 4) was used for both *in vivo* and *in vitro* labeling of purified *Pa* LptD/E_{His} complex and methods reported earlier.[19] After photolabeling, the complex was digested with trypsin, and then analyzed by SDS-PAGE (8% gel) with Western blotting using anti-LptD antibodies, or with detection of biotinylated (photolabeled) proteins by chemiluminescence detection using a streptavidin-HRP conjugate (Figure 5).

MS Analyses. Labeled and unlabeled *Pa* LptD/E_{His} (9 μg) were reconstituted in detergent free 3 M urea in 50 mM ammonium bicarbonate (AmBic) and reduced for 30 min at 37°C with 5 mM TCEP. Each solution was split into three aliquots and proteolytically digested with 0.2 μg lysyl endopeptidase (Lys-C) (*Wako Pure Chemical Industries*) for 14 h at 37°C. Samples were diluted to 1.5 M urea with 50 mM AmBic and further digested for 6 h at 37°C with 0.3 μg sequencing grade modified trypsin (*Promega Corporation*). After dilution to 0.75 M urea with 50 mM AmBic, 0.5 μg chymotrypsin was added for 16 h at 37°C. Samples were acidified to pH < 3 by the addition of formic acid and subjected to C18 purification using 3‑30 μg UltraMicroSpin Columns (*The Nest Group*) according to manufacturer's instructions. HRM calibration peptides (*Biognosys* AG) were added to the samples prior to mass spectrometric analysis.

Peptide samples were separated by reversed-phase HPLC, using a column (75 μm inner diameter, *New Objective*) that was packed in-house with a 15-cm stationary phase (ReproSil-Pur C18-AQ, 1.9 micrometer) and connected to a nano-flow HPLC combined with an autosampler (EASY-nLC II, *Proxeon*). The HPLC was coupled to a Q-Exactive plus mass spectrometer (*Thermo Scientific*) equipped with a nano electrospray ion source (*Thermo Scientific*). Peptides were loaded onto the column with 100% buffer A (99.9% H_2O, 0.1% formic acid (FA)) and eluted for MS detection at a constant flow rate of 300 nL/min with a 70-

min linear gradient from 6–28% buffer B (99.9% MeCN, 0.1% FA) and 4 min 28–50% B. After the gradient, the column was washed 4 min with 98% buffer B. In between runs, the column was cleaned for 18 min with two steep consecutive gradients of MeCN (10–98%). Electrospray voltage was set to 1.8 kV, sheath and auxiliary gas flow to zero and capillary temperature to 250°C.

Samples were first subjected to MS analysis in data-dependent acquisition (DDA) mode for comprehensive and discovery-driven detection of proteolysis derived LptD/E_{His} peptides. In DDA mode, the mass spectrometer automatically switched between MS and MS/MS detection. Following a high-resolution survey mass scan (from 300 to 1,700 m/z) acquired in the Orbitrap with resolution R = 70,000 at 200 m/z (automatic gain control target value $1*10^6$), the 15 most abundant peptide ions with a minimum intensity of 420 were selected for subsequent HCD fragmentation with an isolation window of 1.5 Da and fragments were detected by MS/MS acquisition at resolution R = 35,000 (automatic gain control target value $5*10^4$). Target ions already selected for fragmentation were dynamically excluded for 30 s. Next, samples were analyzed by MS in data-independent acquisition (DIA) mode for the sensitive relative quantification of LptD/E_{His} peptides between **PAL6** labeled and unlabeled condition. Each DIA cycle consists of one full mass scan from 400 to 1220 m/z at resolution R = 35,000 (automatic gain control target value $5*10^6$) followed by 19 sequential DIA MS/MS scans with isolation windows varying between 24 and 220 Da and resolution R = 35,000 (automatic gain control target value $3*10^6$).

Fragment ion spectra acquired in DDA mode were matched against a protein database containing LptD and LptE amino acid sequences in an iterative SEQUEST HT search using Proteome Discoverer v.2.1 (*Thermo Scientific*). First iteration assumed peptides to be fully digested by trypsin with a maximum of 2 missed cleavage sites, followed by searching for fully chymotrypsin cleaved peptides with a maximum of 2 missed cleavages and semi-tryptic ones with a maximum of 2 missed cleavage sites. For all iterations, the precursor and fragment mass tolerance was set to 20 ppm and 0.02 Da, respectively, and methionine oxidation was set as dynamic modification. Identified peptide spectrum matches were filtered for FDR < 1% and exported as spectral library together with common contaminants and standards using Spectronaut v9.0 (*Biognosys* AG) (see Supporting Information). Raw files of mass spectrometry analysis in DIA mode were loaded into Spectronaut. Peptides were identified using above generated spectral library and quantified based on chromatographic traces of

corresponding fragment ions (Table S2). Differential abundance testing was performed at stripped peptide sequence level. LptD/E peptides with an abundance fold change of at least 1.5 and an adjusted p-value (q-value) of < 0.05 were considered to be crosslinked with PAL6 (Figure 6). Obtained peptide variants were mapped to parental LptD/E sequences using Protter proteoform visualization tool[33] and Clustal Omega multiple sequence alignment software to identify preferential binding sites of **PAL6** to LptD/E_{His} (Figure S4). Mass spectrometric data were deposited to the ProteomeXchange Consortium (http://www.proteomexchange.org/) via the PRIDE partner repository (data set identifier: PXD008577).

ACKNOWLEDGMENTS

We thank P. Hunziker (Functional Genomics Center Zurich) for proteomics support, M. Urfer, A. Meier and M. Gwerder for technical support, and D. Kahne (Harvard University) for helpful discussions.

SUPPORTING INFORMATION

The Supporting Information is available free of charge on the ACS Publications website at http://pubs.acs.org.

The Supporting Information includes a list of PCR primers used, homology modelling of LptD from *P. aeruginosa*, and list of LptD/E peptides quantified by MS.

AUTHOR INFORMATION

Corresponding author

E-mail: john.robinson@chem.uzh.ch

ORCID

John Robinson: 0000-0001-7857-8556

Author Contributions – G.A., K.Z., L.C.B., J.S. and G.M. performed protein chemistry and photolabeling studies, M.Mondal, H.K. and J.S. performed binding studies, M.Müller and B.W.

conceived and performed mass spectrometry analyses, K.M. performed modeling studies, J.A.R. oversaw biochemical work and wrote the paper. All authors reviewed the results and approved the final version of the paper.

FUNDING SOURCES

The authors thank the Swiss National Science Foundation (SNF_160259 to B.W; Advanced Researchers PA00P3_134194 and Advanced Postdoc.Mobility grant P300P3-147905 to G.M.; and SNF 205320_146381 to J.A.R.) and the ETH Zurich (research grant ETH-30 17-1 to B.W.) for funding.

References

1. (2017) *Global Priority List of Antibiotic-resistant Bacteria to Guide Research, Discovery, and Development of New Antibiotics*. World Health Organization, Geneva, Switzerland
2. Willyard, C. (2017) The drug-resistant bacteria that pose the greatest health threats. *Nature 543*, 15
3. Henderson, J. C., Zimmerman, S. M., Crofts, A. A., Boll, J. M., Kuhns, L. G., Herrera, C. M., and Trent, M. S. (2016) The Power of Asymmetry: Architecture and Assembly of the Gram-Negative Outer Membrane Lipid Bilayer. *Annu. Rev. Microbiol. 70*, 255-278
4. Whitfield, C., and Trent, M. S. (2014) Biosynthesis and export of bacterial lipopolysaccharides. *Annu. Rev. Biochem. 83*, 99-128
5. Okuda, S., Sherman, D. J., Silhavy, T. J., Ruiz, N., and Kahne, D. (2016) Lipopolysaccharide transport and assembly at the outer membrane: the PEZ model. *Nat. Rev. Microbiol. 14*, 337-345
6. Okuda, S., Freinkman, E., and Kahne, D. (2012) Cytoplasmic ATP Hydrolysis Powers Transport of Lipopolysaccharide Across the Periplasm in E. coli. *Science 338*, 1214
7. Simpson, B. W., May, J. M., Sherman, D. J., Kahne, D., and Ruiz, N. (2015) Lipopolysaccharide transport to the cell surface: biosynthesis and extraction from the inner membrane. *Phil. Trans. Roy. Soc. B 370*, 8
8. Freinkman, E., Okuda, S., Ruiz, N., and Kahne, D. (2012) Regulated assembly of the transenvelope protein complex required for lipopolysaccharide export. *Biochemistry 51*, 4800-4806
9. Li, X. J., Gu, Y. H., Dong, H. H., Wang, W. J., and Dong, C. J. (2015) Trapped lipopolysaccharide and LptD intermediates reveal lipopolysaccharide translocation steps across the Escherichia coli outer membrane. *Sci. Rep. 5*, 8
10. Gu, Y. H., Stansfeld, P. J., Zeng, Y., Dong, H. H., Wang, W. J., and Dong, C. J. (2015) Lipopolysaccharide is Inserted into the Outer Membrane through An Intramembrane Hole, A Lumen Gate, and the Lateral Opening of LptD. *Structure 23*, 496-504

11. Laguri, C., Sperandeo, P., Pounot, K., Ayala, I., Silipo, A., Bougault, C. M., Molinaro, A., Polissi, A., and Simorre, J. P. (2017) Interaction of lipopolysaccharides at intermolecular sites of the periplasmic Lpt transport assembly. *Sci. Rep. 7*, srep9715
12. Dong, H. H., Xiang, Q. J., Gu, Y. H., Wang, Z. S., Paterson, N. G., Stansfeld, P. J., He, C., Zhang, Y. Z., Wang, W. J., and Dong, C. J. (2014) Structural basis for outer membrane lipopolysaccharide insertion. *Nature 511*, 52-56
13. Qiao, S., Luo, Q., Zhao, Y., Zhang, X., and Huang, Y. (2014) Structural basis for lipopolysaccharide insertion in the bacterial outer membrane. *Nature 511*, 108-111
14. Botos, I., Majdalani, N., Mayclin, S. J., McCarthy, J. G., Lundquist, K., Wojtowicz, D., Barnard, T. J., Gumbart, J. C., and Buchanan, S. K. (2016) Structural and Functional Characterization of the LPS Transporter LptDE from Gram-Negative Pathogens. *Structure 24*, 965-976
15. Malojcic, G., Andres, D., Grabowicz, M., George, A. H., Ruiz, N., Silhavy, T. J., and Kahne, D. (2014) LptE binds to and alters the physical state of LPS to catalyze its assembly at the cell surface. *Proc. Natl. Acad. Sci. USA 111*, 9467-9472
16. Sperandeo, P., and Polissi, A. (2016) Lipopolysaccharide Transport to the Cell Surface: New Insights in Assembly into the Outer Membrane. *Structure 24*, 847-849
17. Peng, S., Yan, S., Peng, T., Annie, C., Hai, X., Qi, L., and Jianfeng, C. (2017) Antimicrobial AApeptides. *Curr. Top. Med. Chem. 17*, 1266-1279
18. Shi, Y., Teng, P., Sang, P., She, F., Wei, L., and Cai, J. (2016) γ-AApeptides: Design, Structure, and Applications. *Accs. Chem. Res. 49*, 428-441
19. Srinivas, N., Jetter, P., Ueberbacher, B. J., Werneburg, M., Zerbe, K., Steinmann, J., Van der Meijden, B., Bernardini, F., Lederer, A., Dias, R. L. A., Misson, P. E., Henze, H., Zumbrunn, J., Gombert, F. O., Obrecht, D., Hunziker, P., Schauer, S., Ziegler, U., Kach, A., Eberl, L., Riedel, K., DeMarco, S. J., and Robinson, J. A. (2010) Peptidomimetic Antibiotics Target Outer-Membrane Biogenesis in *Pseudomonas aeruginosa*. *Science 327*, 1010-1013
20. Werneburg, M., Zerbe, K., Juhas, M., Bigler, L., Stalder, U., Kaech, A., Ziegler, U., Obrecht, D., Eberl, L., and Robinson, J. A. (2012) Inhibition of Lipopolysaccharide Transport to the Outer Membrane in *Pseudomonas aeruginosa* by Peptidomimetic Antibiotics. *Chembiochem 13*, 1767-1775
21. Schmidt, J., Patora-Komisarska, K., Moehle, K., Obrecht, D., and Robinson, J. A. (2013) Structural studies of ß-hairpin peptidomimetic antibiotics that target LptD in *Pseudomonas* sp. *Bioorg. Med. Chem. 21*, 5806-5810
22. Vetterli, S. U., Moehle, K., and Robinson, J. A. (2016) Synthesis and antimicrobial activity against *Pseudomonas aeruginosa* of macrocyclic β-hairpin peptidomimetic antibiotics containing N-methylated amino acids. *Bioorg. Med. Chem. 24*, 6332-6339
23. Zerbe, K., Moehle, K., and Robinson, J. A. (2017) Protein Epitope Mimetics: From New Antibiotics to Supramolecular Synthetic Vaccines. *Accts. Chem. Res. 50*, 1323-1331
24. Chng, S., Ruiz, N., Chimalakonda, G., Silhavy, T., and Kahne, D. (2010) Characterization of the two-protein complex in Escherichia coli responsible for lipopolysaccharide assembly at the outer membrane. *Proc. Natl. Acad. Sci. USA 107*, 5363-5368
25. Noinaj, N., Mayclin, S., Stanley, A. M., Jao, C. C., and Buchanan, S. K. (2016) From Constructs to Crystals - Towards Structure Determination of beta-barrel Outer Membrane Proteins. *J. Visual. Exp.*, e53245
26. Ruiz, N., Chng, S., Hiniker, A., Kahne, D., and Silhavy, T. (2010) Nonconsecutive disulfide bond formation in an essential integral outer membrane protein. *Proc. Natl. Acad. Sci. USA 107*, 12245-12250

27. Chng, S., Xue, M., Garner, R., Kadokura, H., Boyd, D., Beckwith, J., and Kahne, D. (2012) Disulfide rearrangement triggered by translocon assembly controls lipopolysaccharide export. *Science 337*, 1665-1668
28. Bodelón, G., Palomino, C., and Fernández, L. Á. (2013) Immunoglobulin domains in *Escherichia coli* and other enterobacteria: from pathogenesis to applications in antibody technologies. *FEMS Microbiol. Rev. 37*, 204-250
29. Frey, L., Lakomek, N. A., Riek, R., and Bibow, S. (2017) Micelles, Bicelles, and Nanodiscs: Comparing the Impact of Membrane Mimetics on Membrane Protein Backbone Dynamics. *Angew. Chem. Int. Ed. 56*, 380-383
30. Moehle, K., Kocherla, H., Bacsa, B., Jurt, S., Zerbe, K., Robinson, J. A., and Zerbe, O. (2016) Solution Structure and Dynamics of LptE from *Pseudomonas aeruginosa*. *Biochemistry 55*, 2936-2943
31. Konovalova, A., and Silhavy, T. J. (2015) Outer membrane lipoprotein biogenesis: Lol is not the end. *Phil. Trans. Roy. Soc. B 370*, 10
32. Nouwens, A. S., Cordwell, S. J., Larsen, M. R., Molloy, M. P., DGillings, M., Willcox, M. D. P., and Walsh, B. J. (2000) Complementing genomics with proteomics: The membrane subproteome of Pseudomonas aeruginosa PAO1. *Electrophoresis 21*, 3797-3809
33. Omasits, U., Ahrens, C. H., Müller, S., and Wollscheid, B. (2014) Protter: interactive protein feature visualization and integration with experimental proteomic data. *Bioinformatics 30*, 884-886

Figure legends

Figure 1. The structure and function of a peptidomimetic antibiotic. **A**, Schematic representation of the LPS transport pathway from the bacterial IM to the OM mediated by LptA–G (see text). Structures from PDB files were used for LptA (2R1A) and LptD/E (4Q35). **B**, Structure of the peptidomimetic antibiotic **L27-11**. **C**, Ribbon representation of the X-ray structure of the LptD/E complex from *Shigella flexneri* (PDB 4Q35).

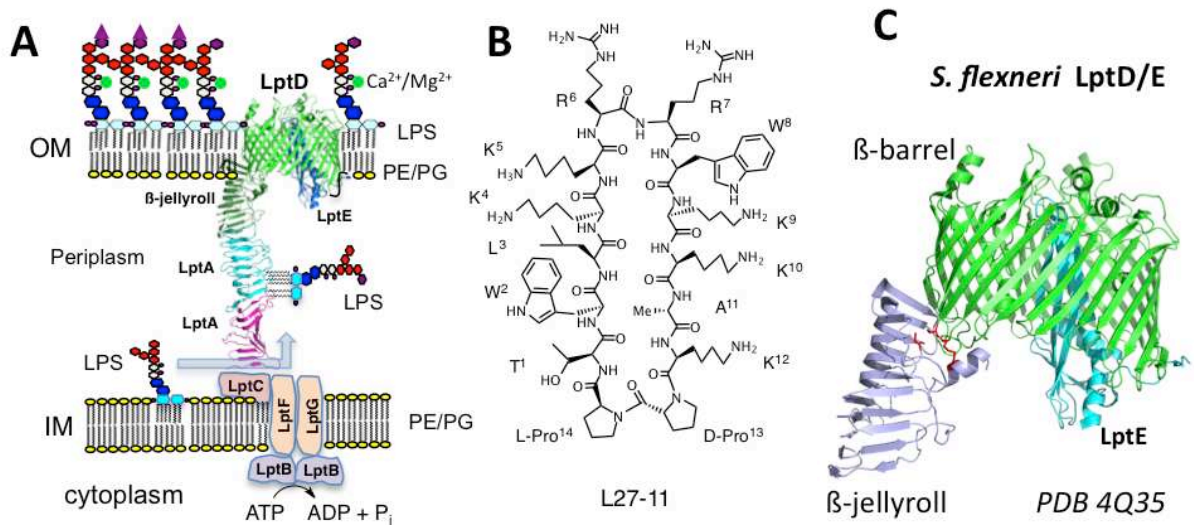

Figure 2. Domain organization and characterization of *Pa* LptD/E$_{His}$. **A**, Comparison of domain organization in LptD from *Pa* (res. 34-924; signal peptide (SP) res. 1-33) and *E. coli* (res. 25-784), and *Pa* LptE$_{His}$. Known Cys-Cys disulfide links in *Ec* LptD are shown in orange (see text). Putative disulfides in *Pa* LptD are shown with dotted lines. The pseudomonas-specific insert domain (predicted res. 45-144) is indicated in orange. **B**, SDS-PAGE of purified *Pa* LptD/E$_{His}$ after heat denaturation and reduction with DTT (positions of LptD and LptE$_{His}$ are indicated). **C**, Western blot showing the mobility in SDS-PAGE after heat denaturation; of *Pa* LptD extracted from *P. aeruginosa* PAO1 membranes (lanes 1), compared to that of LptD/E$_{His}$ isolated from *E. coli* (lanes 2), either with or without reduction by DTT. Detection is with anti-LptD antibodies. **D**, Analysis of *Pa* LptD (wt, from *P. aeruginosa*) and Cys-to-Ser mutants of LptD/E$_{His}$ by Western blotting with anti-LptD antibodies.

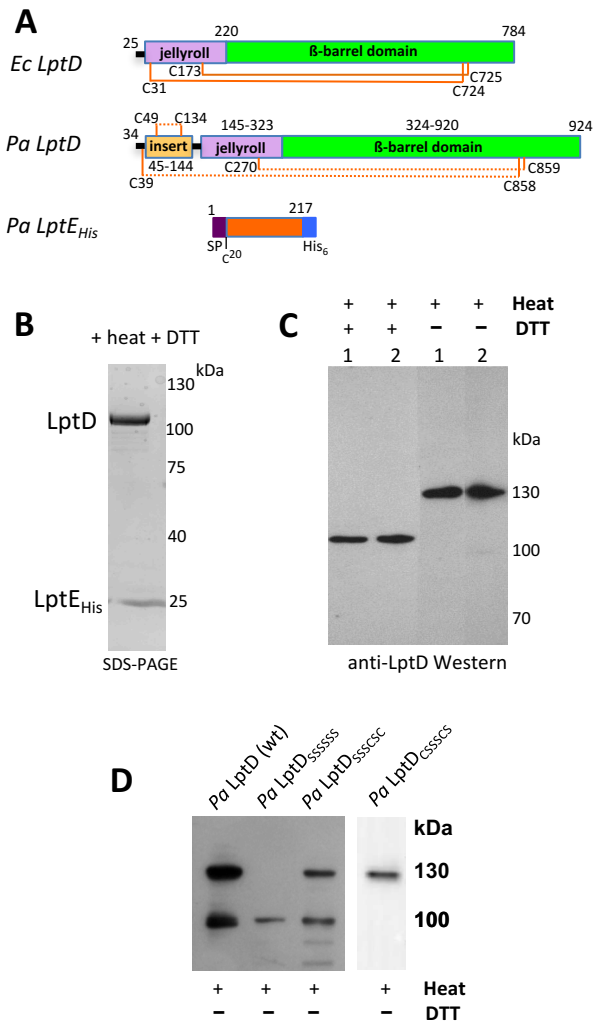

Figure 3. **Binding of antibiotic to LptD/E$_{His}$**. Two independent biophysical methods were used for binding studies; **A**, SPR measurements of **L27-11** binding to *Pa* LptD/E$_{His}$ immobilized on a NiHC1000 biosensor surface (BIAcore T100). Responses are shown for increasing concentrations of **L27-11** (0.25–500 nM) in the flow buffer. A standard Langmuir binding model was used to determine K_D (32 ± 10 nM) from triplicate measurements. **B**, Binding curves from microscale thermophoresis measurements in buffer (see experimental section) with a constant amount of **fl-L27-11** and varying concentrations of *Pa* LptD/E$_{His}$. Three independent experiments are shown (K_D of 13 ± 5 nM).

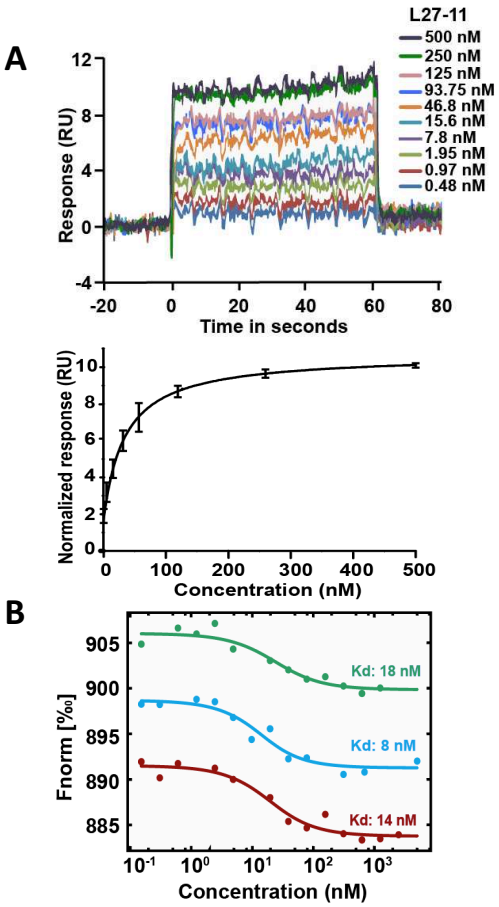

Figure 4. Structures of probes. Structures of the photoprobe **PAL6** and the fluorescent probe (**fl-L27-11**) used for MST binding studies.

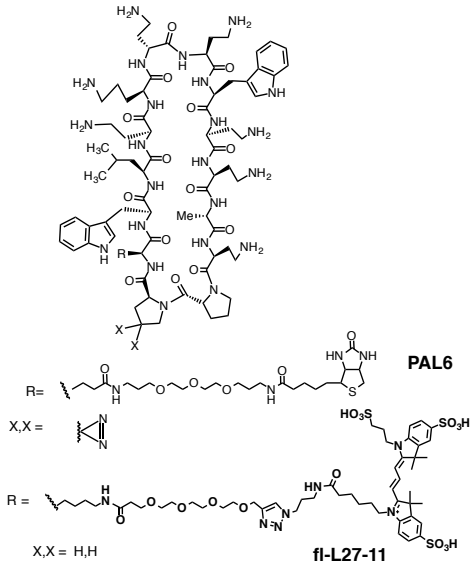

Figure 5. **Photolabeling of *Pa* LptD/E$_{His}$. A**, Partial trypsin digestion of *Pa* LptD/E$_{His}$ (ratio in μg of LptD/E:trypsin shown). LptD after heating and reduction with DTT (≈100 kDa), and trypsin fragments F1 (≈95 kDa) and F2 (70 kDa) are indicated (N-terminal sequences determined by the Edman method are shown). **B**, OM extract of *in vivo* photolabeled *Pa* by Coomassie-stained SDS-PAGE (8% gel), same after blotting and biotin detection, and after anti-LptD detection. With (+) and without (-) trypsin digestion, showing that fragment F1 is not biotin-labeled. **C**, Repeat as in **B** but showing course of trypsin digestion. Lane-1 shows LptD control (Non-labeled, NL). *Top*, anti-LptD Western blot; *bottom*, biotin detection. Intact LptD and fragment F1 are indicated, and again F1 is not biotin-labeled. **D**, *In vitro* photolabeled *Pa* LptD/E$_{His}$ analyzed by Coomassie-stained SDS-PAGE (8% gel) (*left*), and after blotting and biotin detection (*right*); both with (+) or without (-) partial trypsin digestion. Fragment F1 is, and F2 is not biotin-labeled. **E**, As in **D** but showing time course (in min.) of trypsin digestion (μg of LptD/E:trypsin ≈ 50:1). Lane-1 shows LptD control (Non-labeled, NL). *Top*, anti-LptD Western blot; *bottom*, biotin detection. Intact LptD and fragment F1 are indicated.

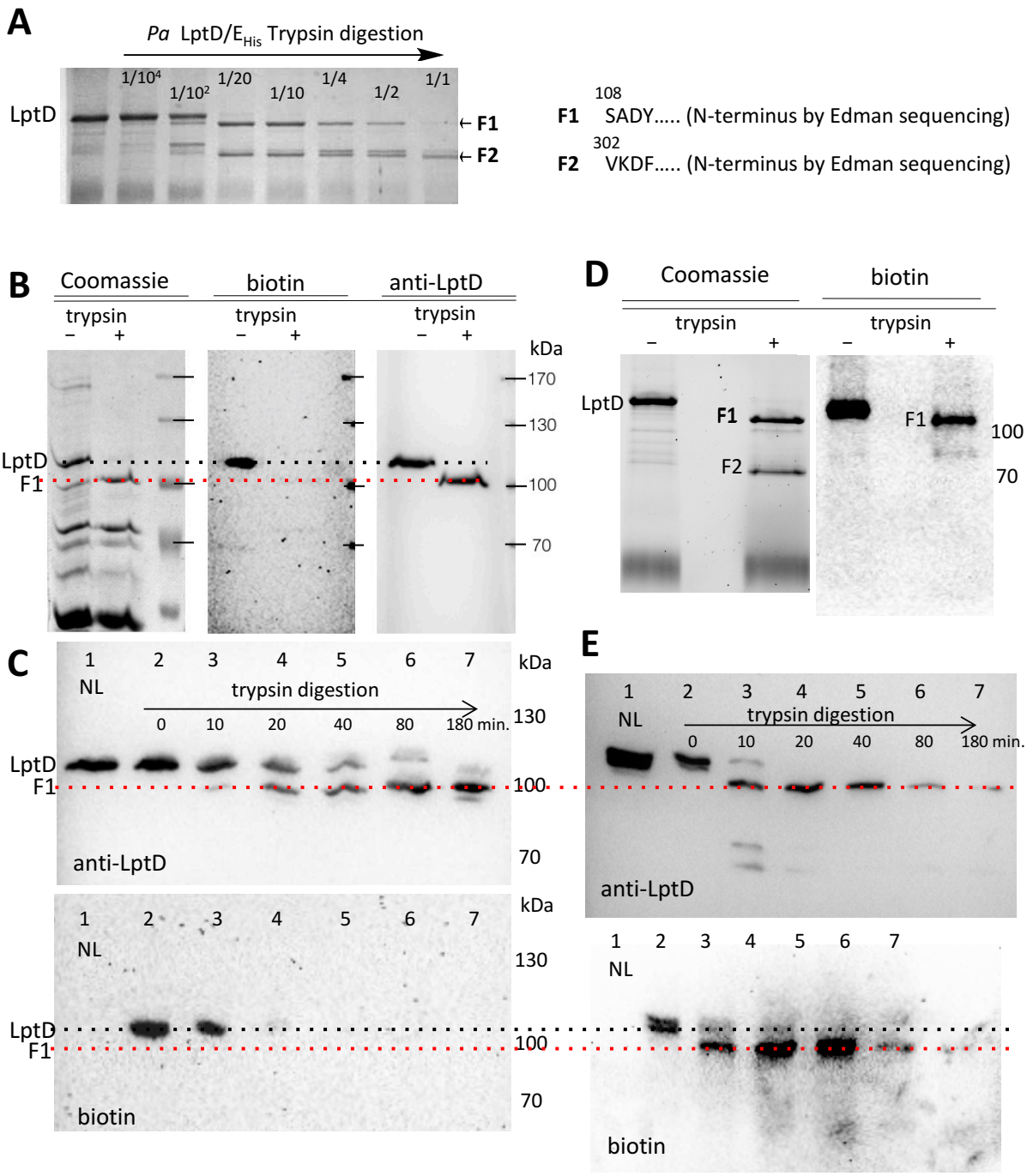
A
Pa LptD/E His Trypsin digestion
1/10^4
1/10^2
1/20
1/10
1/4
1/2
1/1
LptD
F1
F2
F1 108 SADY..... (N-terminus by Edman sequencing)
F2 302 VKDF..... (N-terminus by Edman sequencing)
B
Coomassie
biotin
anti-LptD
trypsin
kDa
170
130
100
70
LptD
F1
C
NL
trypsin digestion
0 10 20 40 80 180 min.
anti-LptD
biotin
D
Coomassie
biotin
F2
E

Figure 6. Volcano plot showing depletion of proteolytic peptide fragments from LptD by *in vitro* photolabeling with PAL6. **A**, Peptide fragments from photolabeled and unlabeled LptD were quantified by MS-based proteomics and the fold change calculated. Peptides with an abundance change of larger than ±1.5 fold and q-value <0.05 were considered as significantly regulated by photolabeling. Regulated peptides derived from the **insert domain (orange, triangles)**, **ß-jellyroll (purple, squares)** and **ß-barrel domain (green circles)** of LptD are depicted. Significantly downregulated peptides of the insert and beta jellyroll domain share a unique amino acid sequence ETV (res. 85–87) and ENR (res. 199–201), respectively. **B**, List of the significantly depleted peptide fragments of the LptD insert and ß-jellyroll domains (orange and purple) as quantified by MS. The ETV and ENR sequence motifs are highlighted in bold.

A

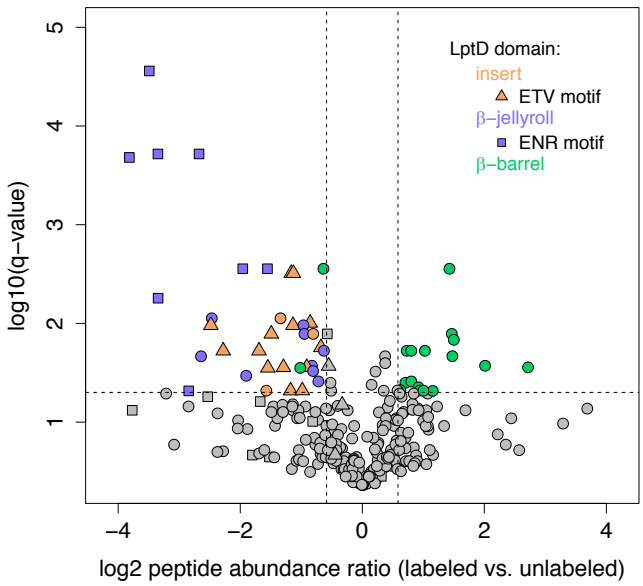

B

List of significantly downregulated peptides identified by MS:

LptD domain	Sequence	LptD domain	Sequence
insert	SVSTAAAGSSVSGSGG**ETV**EAEPTQR	β-jellyroll	DESPTYVSAK
insert	AAAGSSVSGSGG**ETV**EAEPTQR	β-jellyroll	TLAGDVVLR
insert	AAGSSVSGSGG**ETV**EAEPTQR	β-jellyroll	QGSMQVEGDEANLH
insert	AGSSVSGSGG**ETV**EAEPTQR	β-jellyroll	GSMQVEGDEANLHQL**ENR**
insert	GSSVSGSGG**ETV**EAEPTQR	β-jellyroll	QVEGDEANLHQL**ENR**
insert	SSVSGSGG**ETV**EAEPTQR	β-jellyroll	QVEGDEANLHQL**ENR**GELVGNVK
insert	SVSGSGG**ETV**EAEPTQR	β-jellyroll	VEGDEANLHQL**ENR**GELVGNVK
insert	VSGSGG**ETV**EAEPTQR	β-jellyroll	GDEANLHQL**ENR**GELVGNVK
insert	SGSGG**ETV**EAEPTQR	β-jellyroll	DEANLHQL**ENR**GELVGNVK
insert	GSGG**ETV**EAEPTQR	β-jellyroll	QL**ENR**GELVGNVK
insert	SGG**ETV**EAEPTQR	β-jellyroll	**ENR**GELVGNVK
insert	GG**ETV**EAEPTQR	β-jellyroll	NRGELVGNVK
insert	G**ETV**EAEPTQR	β-jellyroll	GMLVVGDHAQVQ
insert	**ETV**EAEPTQR	β-jellyroll	RSENAIIM
insert	RSADYSHLDWIPREK	β-jellyroll	RSENAIIMLK
insert	SADYSHLDWIPREK	β-jellyroll	SENAIIMLK
insert	SHLDWIPREK	β-jellyroll	ENAIIMLK

Figure 7. Representation of *Pa* LptD/E. **A**, Structure of LptD/E, with the LptD N-terminus, insert domain and jellyroll domain shown schematically, since no 3D structural information is available for the periplasmic segment of *Pa* LptD (see Figure 1C and 2A). The connectivity of the protein suggests that the insert, jellyroll and ß-barrel domains will be in close proximity to each other, but their relative orientations are presently unknown. **B**, A homology model of the *Pa* LptD jellyroll domain is shown, with res. 199–201 (*cyan*) and the site of mutation conferring antibiotic resistance (res. 210–215, *yellow*) indicated (see text).